Cell Reports

Recovery of consolidation after sleep following stroke—interaction of slow waves, spindles, and GABA

Graphical abstract

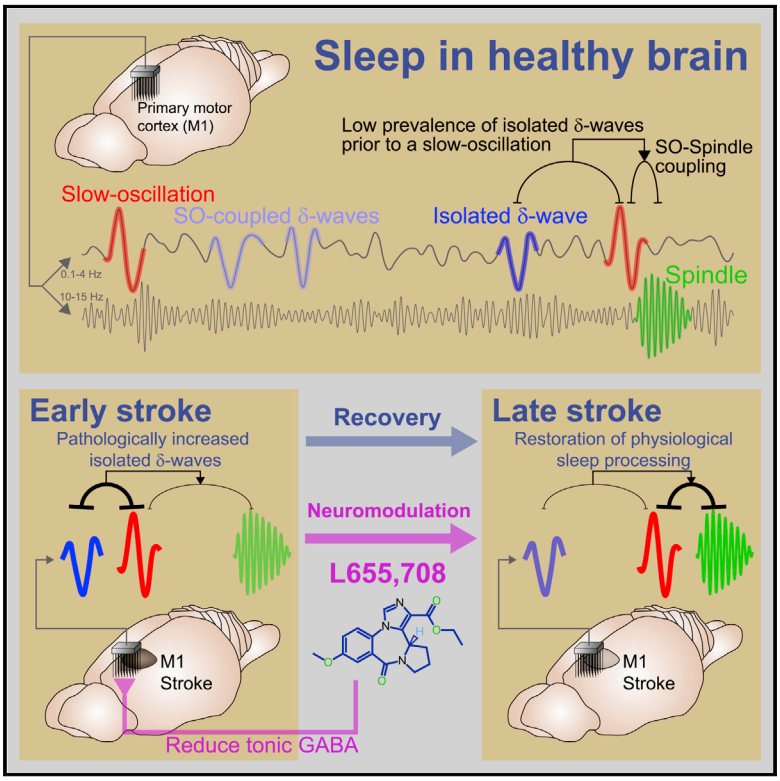

Highlights

- SO-spindle coupling is impaired after stroke and recovers with motor training
- Isolated local delta waves pathologically increase during sleep after stroke
- Post-stroke sleep processing is impaired due to an increase in local delta waves
- Reduction of inhibition transitions sleep after stroke to a more physiological state

Authors

Jaekyung Kim, Ling Guo, April Hishinuma, Stefan Lemke, Dhakshin S. Ramanathan, Seok Joon Won, Karunesh Ganguly

Correspondence

seokjoon.won@va.gov (S.J.W.), karunesh.ganguly@ucsf.edu (K.G.)

In brief

Kim et al. reveal that motor recovery after stroke is associated with both increased coupling of spindle to slow oscillations and decrease of pathologically isolated delta waves. Such changes can be modulated by reduction of tonic GABAergic inhibition. These highlight the potential importance of sleep-associated processing for enhancing motor recovery after stroke.

Kim et al., 2022, Cell Reports *38*, 110426
March 1, 2022
https://doi.org/10.1016/j.celrep.2022.110426

Cell Reports

CellPress
OPEN ACCESS

Report

Recovery of consolidation after sleep following stroke—interaction of slow waves, spindles, and GABA

Jaekyung Kim,[1,2] Ling Guo,[1,2] April Hishinuma,[1,2] Stefan Lemke,[1,2] Dhakshin S. Ramanathan,[1,2,3,4] Seok Joon Won,[1,2,*] and Karunesh Ganguly[1,2,5,*]

[1]Neurology and Rehabilitation Service, San Francisco Veterans Affairs Medical Center, 1700 Owens Street, San Francisco, CA 94158, USA
[2]Department of Neurology, University of California, San Francisco, San Francisco, CA 94158, USA
[3]Present address: Mental Health Service, VA San Diego Health System, San Diego, CA, USA
[4]Present address: Department of Psychiatry, University of California, San Diego, San Diego, CA, USA
[5]Lead contact
*Correspondence: seokjoon.won@va.gov (S.J.W.), karunesh.ganguly@ucsf.edu (K.G.)
https://doi.org/10.1016/j.celrep.2022.110426

SUMMARY

Sleep is known to promote recovery after stroke. Yet it remains unclear how stroke affects neural processing during sleep. Using an experimental stroke model in rats along with electrophysiological monitoring of neural firing and sleep microarchitecture, here we show that sleep processing is altered by stroke. We find that the precise coupling of spindles to global slow oscillations (SOs), a phenomenon that is known to be important for memory consolidation, is disrupted by a pathological increase in "isolated" local delta waves. The transition from this pathological to a physiological state—with increased spindle coupling to SO—is associated with sustained performance gains during recovery. Interestingly, post-injury sleep could be pushed toward a physiological state via a pharmacological reduction of tonic γ-aminobutyric acid (GABA). Together, our results suggest that sleep processing after stroke is impaired due to an increase in delta waves and that its restoration can be important for recovery.

INTRODUCTION

Stroke is a leading cause of motor disability; despite advancements in rehabilitation, there are no widely used therapies to augment plasticity and improve function (Ganguly et al., 2013; Macdonell et al., 1988; Norrving and Kissela, 2013). Importantly, it is now clear that a major function of sleep is to regulate neuroplasticity (de Vivo et al., 2017; Genzel et al., 2014; Gulati et al., 2015, 2017; Helfrich et al., 2018; Kim et al., 2019; Klinzing et al., 2019; Latchoumane et al., 2017; Ramanathan et al., 2015; Stickgold, 2005; Tononi and Cirelli, 2014; Yang et al., 2014). Thus, optimizing sleep processing during rehabilitation has the great potential to enhance recovery. While both clinical and preclinical studies of stroke have demonstrated that sleep can influence motor recovery after stroke (Backhaus et al., 2018; Baumann et al., 2006; Duss et al., 2017; Facchin et al., 2020; Gao et al., 2010; Giubilei et al., 1992; Gottselig et al., 2002; Poryazova et al., 2015; Siengsukon and Boyd, 2009), it remains unclear precisely how sleep processing is affected by stroke.

In general, sleep-dependent processing has been closely linked to memory consolidation or the process of transforming newly encoded information into more stable long-term memories (Born et al., 2006; Stickgold, 2005). While consolidation is most studied for hippocampal-cortical interactions (Ito et al., 2015; Molle et al., 2006; Rothschild et al., 2017; Sirota et al., 2003), sleep is also known to benefit motor memories (Kim et al., 2019; Korman et al., 2007; Lemke et al., 2021; Walker et al., 2002). Specifically, non-rapid eye movement (NREM) sleep is associated with reactivation of neural ensembles linked to movement control and performance gains after sleep (termed "offline" gains; Gulati et al., 2017; Kim et al., 2019; Ramanathan et al., 2015). Notably, memory consolidation is known to require the precise coupling of sleep spindles to global slow waves, i.e., slow oscillations (SOs) (Born et al., 2006; Buzsáki, 2015; Cairney et al., 2018; Helfrich et al., 2018; Kim et al., 2019; Latchoumane et al., 2017; Maingret et al., 2016; Ngo et al., 2013). Thus, a key goal of this study was to characterize how sleep oscillations are affected by an experimentally induced focal cortical stroke and how their characteristics may influence recovery of sleep-associated gains in task performance, i.e., consolidation.

What might be the features of sleep that are altered by an experimentally induced stroke? Recent work has shown that the balance between global SOs and local slow waves—delta waves (δ)—determines whether there is an enhancement of skill or, instead, forgetting (Kim et al., 2019). Intriguingly, recordings in stroke patients (Poryazova et al., 2015; Sarasso et al., 2020; Tu-Chan et al., 2017; van Dellen et al., 2013) and in animal models of stroke (Burns, 1951; Burns and Webb, 1979; Carmichael and Chesselet, 2002; Gulati et al., 2015; Nita et al., 2007) have found a prevalence of *local* low-frequency power (<4 Hz) during awake periods; this also appears to be far more common after a cortical than a subcortical lesion (Macdonell et al., 1988).

Intriguingly, δ waves may also be apparent in sleep periods after stroke (Poryazova et al., 2015). Together, these observations suggest the possibility that the sleep microarchitecture after a cortical stroke might contain more δ waves relative to SO, thereby impairing sleep-associated "strengthening" of memory, i.e., bias sleep processing toward a "forget" state.

Here, we demonstrate that, after induction of an experimental cortical stroke, the sleep microarchitecture of the perilesional cortex (PLC) is altered such that there is a reduced coupling of sleep spindles to SOs. With the recovery of motor function, there was a redistribution of sleep spindles toward a more physiological state, characterized by an increase in precise spindle-SO coupling and stronger post-training offline gains after sleep. We also found that there was a concomitant reduction in local δ waves. Interestingly, there was a direct correlation between the rate of local δ waves and the precise coupling of spindles to SOs. Remarkably, the post-stroke imbalance between δ waves and SO could be modulated by a pharmacological treatment that reduced $GABA_A$-mediated tonic inhibition (Clarkson et al., 2010). Together, our results suggest that restoration of sleep processing may allow animals to build upon daily training and allow sustained offline performance gains.

RESULTS

Changes in spindle-SO nesting over recovery

We used a focal cortical stroke model ($stroke_{exp}$) (Clarkson et al., 2010; Ramanathan et al., 2018; Roome et al., 2014) to examine alterations in NREM sleep microarchitecture during recovery (Figure 1A); we implanted microelectrode arrays in the premotor cortex (i.e., PLC; n = 8; Table S1). We measured retrieval success in a single pellet task (Figures 1B and S1A); this reach-to-grasp task is a sensitive measure of prehension (Guo et al., 2021; Ramanathan et al., 2018; Whishaw et al., 1986; Wong et al., 2015). The first monitored session was 1 to 2 weeks after $stroke_{exp}$ (STAR Methods). Each animal experienced task training for 6–11 sessions over a period of 2 to 3 weeks (performance in Figure S1B). Given the variability of recovery, each animal's sessions were divided into tertiles, "early," "middle," and "late." We first focused on the "pre-training" sleep (sleep immediately prior to training); SO, δ waves, and spindles were identified using the filtered local field potential (LFP) (Figure 1C; STAR Methods). Sleep was detected using video analysis, and NREM sleep was detected using power spectral density (Figure S1C; STAR Methods; Kim et al., 2019). We examined changes in temporal interactions of spindles to SOs within the pre-training sleep. The pre-training sleep likely reflects general changes in sleep microarchitecture and is unlikely to reflect the immediate consequence of task training.

In the healthy brain, nesting of spindles to SOs is known to be essential for consolidation (Antony et al., 2018; Bergmann and Born, 2018; Cairney et al., 2018; Helfrich et al., 2018; Kim et al., 2019; Latchoumane et al., 2017; Maingret et al., 2016; Ngo et al., 2013; Staresina et al., 2015). It also is important for triggering offline gains (Kim et al., 2019; Lemke et al., 2021; Ramanathan et al., 2015; Silversmith et al., 2020). We thus focused on comparing the "nesting" of spindles to SOs in the PLC (Figure 1D; STAR Methods). More specifically, we measured temporal lags between an SO and its nearest spindle ($\Delta T_{SO\text{-}Spindle}$). With recovery, SO nesting became more probable (Figure 1E) and the distribution of $\Delta T_{SO\text{-}Spindle}$ became sharper, indicating spindles were occurring closer to SOs (Figure 1F). Furthermore, from the distribution of $\Delta T_{SO\text{-}Spindle}$, the SO nesting was quantified by the probability of spindles within the nesting window (Figure 1F, gray box; −0.5–1 s from SO up states). SO nesting significantly increased over the period of motor recovery (Figure 1G). Moreover, there was a strong increase in SO nesting in the late compared with the early period (Figure 1H). We also examined the rates of SO-nested spindles and found a significant increase in the late compared with the early period (early, n = 16 sessions in eight rats, 10.1 ± 0.60 count/min versus late, n = 16 sessions in eight rats, 12.3 ± 0.63 count/min, linear mixedeffects model (LME); t_{30} = 2.52; p = 0.017; Figure S2). Notably, there was a significant positive relationship between the restoration of SO nesting and improvements in task performance (Figure 1B versus Figure 1G; LME fit; R = 0.38; p = 0.031). Interestingly, SO-nested spindles were also associated with a significantly stronger spike modulation depth (MD) and spindles amplitudes at the late versus the early period (MD, Figure 1I; amplitude: LME; t_{30} = 2.26; p = 0.031). Taken together, these results indicate a change in the precise temporal coupling of spindles and SOs during recovery.

Changes in sleep microarchitecture after task training

We wondered how task training affected the sleep microarchitecture. Past work has shown that task training in the healthy brain can induce short-term changes in spindle-SO coupling, i.e., short-term "reactive" effects after training (Figure 2A). Interestingly, we found that sessions in the late period demonstrated greater increases in spindle-SO nesting following training compared with the early period (Figure 2B). The rate of SO-nested spindles did not change (early versus late; LME; t_{30} = 1.27; p = 0.21; Figure S2). When we examined within-session changes in task performance (Figures 1A and 2A), we found a significant trend in the correlation between changes in SO nesting and offline gains (LME fit; R = 0.28; p = 0.049). Interestingly, changes in SO nesting were more clearly linked to changes in task performance the following day (LME fit; R = 0.80; p = 0.045; Figure 2C). In other words, with continued recovery time after $stroke_{exp}$, motor training appeared to be able to trigger reactive changes in the subsequent sleep period; this appeared to manifest as improved performance the following day. This is consistent with findings that a full night of sleep results in changes in functional connectivity (Lemke et al., 2021).

Is it also possible that there is a direct relationship between sleep duration and offline gains? We performed experiments in separate groups with $stroke_{exp}$ to test this (Figures 2D and 2E). We specifically assessed the effects of sleep duration on offline gains during *middle-late phase* of recovery, i.e., when each animal demonstrated performance improvements. In other words, we did not use *early* period linked to abnormal sleep activity. In this separate group, we measured the effects of sleep on the task and compared these with a sleep restriction group (Figure 2D). For the sleep group (sleep: n = 29 sessions in six rats), we measured sleep duration using video-based detection.

CellPress
OPEN ACCESS

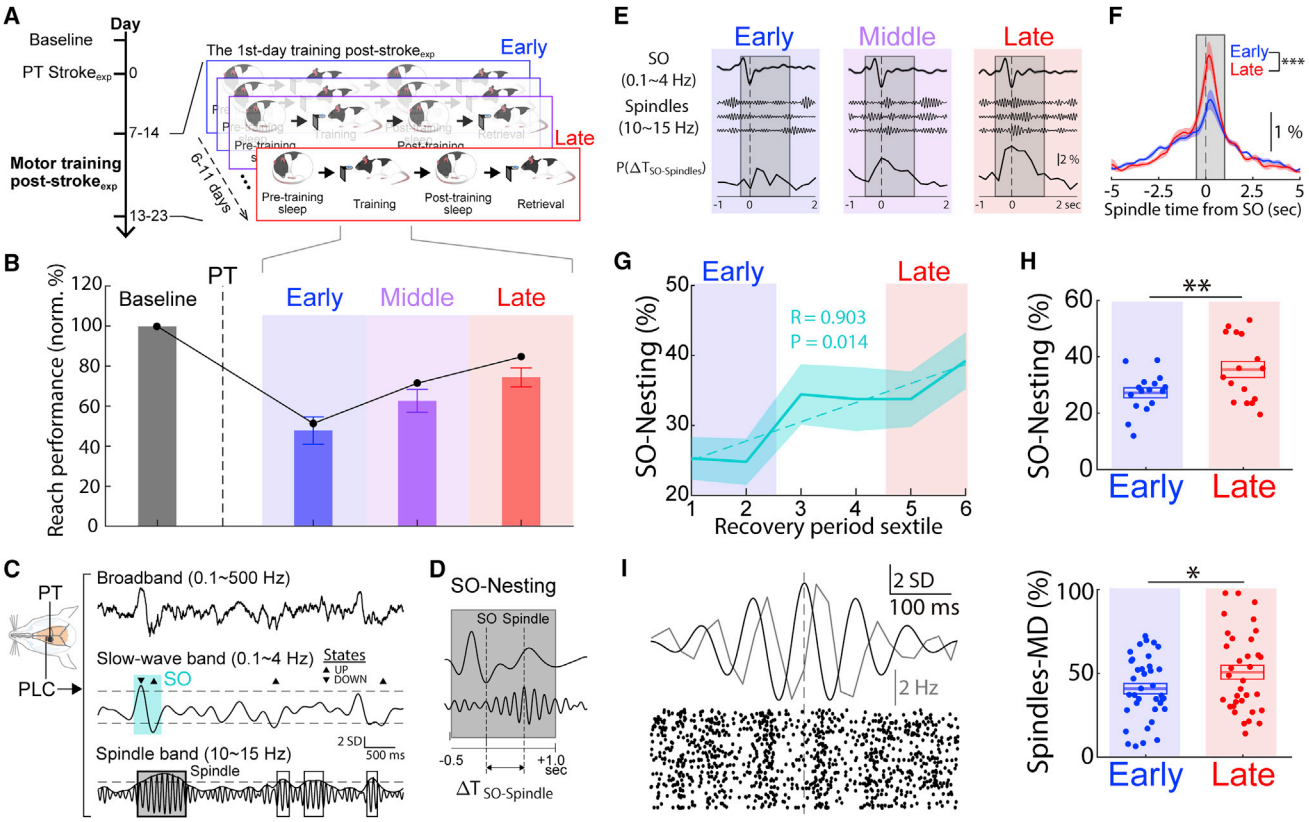

Figure 1. Reach performance and redistribution of spindles toward SO over recovery

(A) Experimental flow. PT, photothrombotic stroke$_{exp}$.

(B) Mean retrieval success rates (n = 8 rats; black dots: two-session average per period for single animal). Bars show average of sessions in tertiles. Mean ± SEM.

(C) Examples of broadband (0.1–500 Hz) and filtered (0.1–4 Hz SO; 10–15 Hz spindles) trace in PLC. SO, cyan; spindle, gray. Open boxes show non-spindle events.

(D) Cartoons of SO nesting. Nesting window −0.5–1.0 s from SO up state is shown (same as E and F).

(E) Examples of SO-spindle interaction. Mean SO-up-state-triggered LFP is shown. Three single-trial examples of detected spindles near SOs (middle) are shown. Examples of probability distribution (bottom) are shown.

(F) Comparison in distributions of $\Delta T_{SO\text{-}Spindles}$ between early and late (n = 16 sessions, eight rats; Bartlett's test, $\chi^2 = 58.7$, ***$p < 10^{-13}$).

(G) Average time courses of SO nesting and δ_l nesting over recovery (n = 8 rats). Dashed is linear regression (R = 0.903; p = 0.014). Mean ± SEM.

(H) SO nesting early versus late (early, n = 16 sessions in eight rats, 27.2% ± 1.7% versus late, n = 16 sessions in eight rats, 35.5% ± 2.8%, LME, $t_{30} = 3.58$, **p = 0.011; using averages per period, early, n = 8 rats, 27.2% ± 2.4% versus late, n = 8 rats, 35.5% ± 3.5%, LME, $t_{14} = 3.58$, **p = 3.0×10^{-3}). Mean ± SEM.

(I) (Left) Average of event-triggered LFP (10–15 Hz; black), spike rates (gray), and raster plot of an example unit. (Right) Unit modulation depth (MD) during spindles for early (n = 37 units, eight rats; 40.9% ± 3.1%) and late (n = 34 units, eight rats; 50.7% ± 4.1%) is shown. There were significant changes from early to late (LME; $t_{69} = 2.21$; *p = 0.030). Mean ± SEM.

In the restriction group (no-sleep: n = 28 sessions in eight rats), sleep was restricted either 2–6 h after training and then the retrieval was conducted. The rats with post-training sleep experienced greater offline gains in task performance in comparison to the sleep-restricted animals (sleep: 6.4% ± 1.8% versus no-sleep: −2.5% ± 2.3%; two-sample t test; $t_{55} = 2.28$; p = 0.027). We also found a significant relationship between sleep duration and task performance in the middle-late period (LME fit; R = 0.52; p = 0.022; Figure 2E); however, there was no significant relationship when including the early phases of recovery (LME fit; R = 0.25; p = 0.25). We interpreted these results to mean that sleep-associated processing might be beneficial after an initial early phase. Together, these results suggest a precise dose-outcome relationship between sleep duration and gains.

Pathological local δ waves

We next examined changes in the temporal interactions of δ waves with SOs and spindles. For the pre-training sleep shown in Figure 1, δ waves were also identified using the filtered LFP at 0.1–4 Hz (Figure 3A; STAR Methods). We then measured the temporal relationship between δ waves and SO ($\Delta T_{SO\text{-}\delta}$) in two groups of rats (photothrombotic [PT] stroke$_{exp}$ in M1, n = 8 rats and healthy rats, n = 5; Figure 3B). In healthy animals, δ waves typically follow SOs. We then compared it with the early period after stroke$_{exp}$. Interestingly, in the early period, there was a significant increase in δ waves that were apparently decoupled from SOs, i.e., temporally far from the previous SOs. All stroke$_{exp}$ animals demonstrated this effect compared with healthy animals (Figure 3C). Using the 50th percentile of this distribution, we

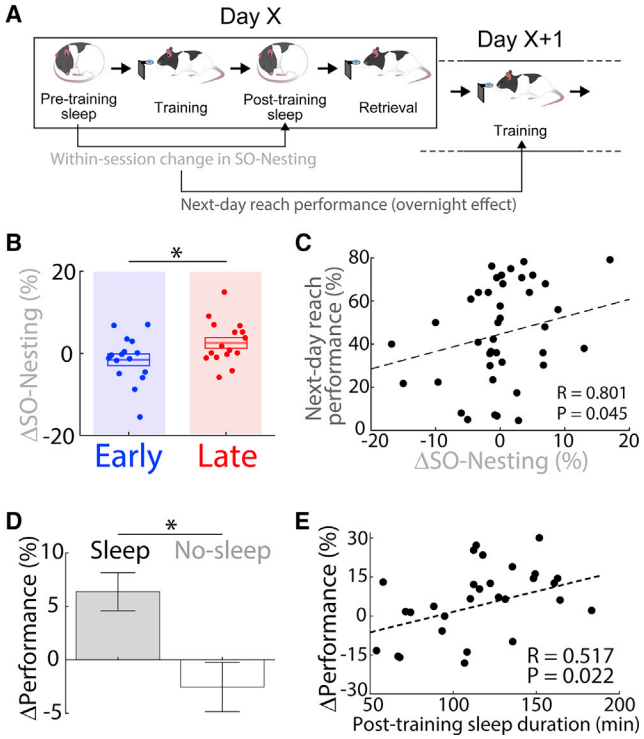

Figure 2. Spindle redistribution and offline gains

(A) Within-session changes (i.e., changes in day X) of SO nesting compared with next-day (day X+1) performance.

(B) Comparison of changes in the SO nesting within a session (ΔSO nesting: early, n = 16 sessions in eight rats, −1.6% ± 1.4% versus late, n = 16 sessions in eight rats, 2.6% ± 1.3%; LME; $t_{30} = 2.24$; *p = 0.032). Mean ± SEM.

(C) Relationship of ΔSO nesting to the next-day performance over recovery (LME fit, R = 0.801, p = 0.045; n = 40 sessions in eight rats, five pairs per animal).

(D) Within-session changes in the motor performance (Δperformance; changes from reach training to retrieval) during the recovery $_p$ (sleep, n = 29 sessions in six rats: 6.4% ± 1.8%; no-sleep, n = 28 sessions in eight rats: −2.5% ± 2.3%; sleep versus no-sleep, LME, $t_{55} = -2.31$, *p = 0.024). Mean ± SEM.

(E) Relationship of post-training sleep duration to changes in performance (LME fit; R = 0.517; p = 0.022).

separated δ waves into two classes, "SO-coupled (δ_{SO})" and "isolated (δ_I)" (STAR Methods). Notably, the overall ratios of SO/δ were similar in both stroke$_{exp}$ and healthy animals (stroke$_{exp}$: 27.9% ± 2.2% versus healthy: 32.4% ± 2.6%; two-sample t test; $t_{23} = -1.31$; p = 0.24). Thus, after stroke$_{exp}$, while the relative number of SOs and δ waves were comparable to the healthy state, there was a significant increase in the prevalence of δ_I waves not temporally coupled to an SO. We also examined changes in the temporal interactions of spindles to δ_I waves in the PLC. We analyzed "δ_I nesting" in a similar manner to SO nesting, i.e., its closest spindle (Figure 3D; STAR Methods). With recovery, δ_I nesting significantly decreased over recovery (Figure 3E). Moreover, there was a moderate decrease in the late compared with the early period (Figure 3F). We also examined the rates of δ_I-nested spindles and found no significant change (early, n = 16 sessions in eight rats, 10.3 ± 0.70 count/min versus late, n = 16 sessions in eight rats, 11.1 ± 0.51 count/min; LME; $t_{30} = 1.18$; p = 0.25; Figure S2). Notably, there was a negative relationship between the decrease of δ_I nesting and time-dependent improvements in task performance (Figure 1B versus Figure 3E; LME fit; R = −0.43; $p < 10^{-2}$). The relative nesting, i.e., SO nesting/δ_I nesting was more predictive of recovery compared with SO nesting (SO nesting/δ_I nesting: LME fit; R = 0.46; $p < 10^{-2}$; smaller absolute errors between true and predicted performances by SO nesting/δ_I nesting versus SO nesting: paired t test; $t_{31} = 2.18$; p = 0.037). Together, these results indicate there was a change in the precise temporal coupling of spindles toward SOs and away from δ_I waves with recovery.

Relationship between local δ_I waves preceding SO and nesting

Is there a more direct relationship of these observed changes in δ_I waves on SO-spindle nesting? Past studies have shown that changes in SO parameters (e.g., amplitude) can depend on the temporal proximity of slow waves (Bernardi et al., 2018; Ngo et al., 2015). Given the changes we observed in SO nesting with recovery, we examined whether changes in how often δ_I waves directly preceded an SO event could predict this. We examined how many δ_I waves preceded SOs, i.e., −5–0 s from SO up state (Figure 3G). Remarkably, this appeared to significantly influence spindle nesting to SO; we found a strong negative correlation between the δ_I wave rate preceding SOs and SO nesting (Figure 3H). Furthermore, the rate of δ_I waves preceding SOs had a significant negative correlation with the task performance the following day (Figure 3I) as well as the within-session changes in task performance (LME fit; R = 0.30; p = 0.032). Thus, our results suggest that the prevalence of δ_I waves in the early phase can influence the nesting of spindles to SOs and changes in performance.

Reducing elevated tonic inhibition and pathological sleep

What might be the underlying neurophysiological basis for our observed changes in SO and δ_I waves with recovery? One possibility is that elevations in extra-synaptic γ-aminobutyric acid (GABA) after stroke$_{exp}$ may alter local excitability and thus perturb the ability of global SOs to organize local δ. Studies have reported that reducing such tonic inhibition can have a beneficial effect on recovery (Clarkson et al., 2010; He et al., 2019), implying that altered excitation-inhibition (E-I) balance (Kim and Fiorillo, 2017; Xia et al., 2017; Yizhar et al., 2011) plays a role in recovery.

We tested the effects of blocking $GABA_A$ tonic inhibition after stroke$_{exp}$ on the coupling of spindles to slow waves. For these experiments, we only tested this intervention during the early spontaneous recovery period; this allows us to examine changes in the absence of contributions from task training. We injected the $GABA_A$ α5-subtype receptor inverse agonist (L655-708; Clarkson et al., 2010) during early recovery after a PT stroke$_{exp}$ (n = 3 rats) or endothelin-1 (ET-1) stroke$_{exp}$ (n = 3 rats). The ET-1 approach allowed us to collect baseline neural data prior to stroke induction (STAR Methods). This was followed by recordings after the injection of vehicle (sham) or L655-708 (drug) during early recovery, i.e., days 7–12 after stroke$_{exp}$ (Figure 4A).

CellPress
OPEN ACCESS

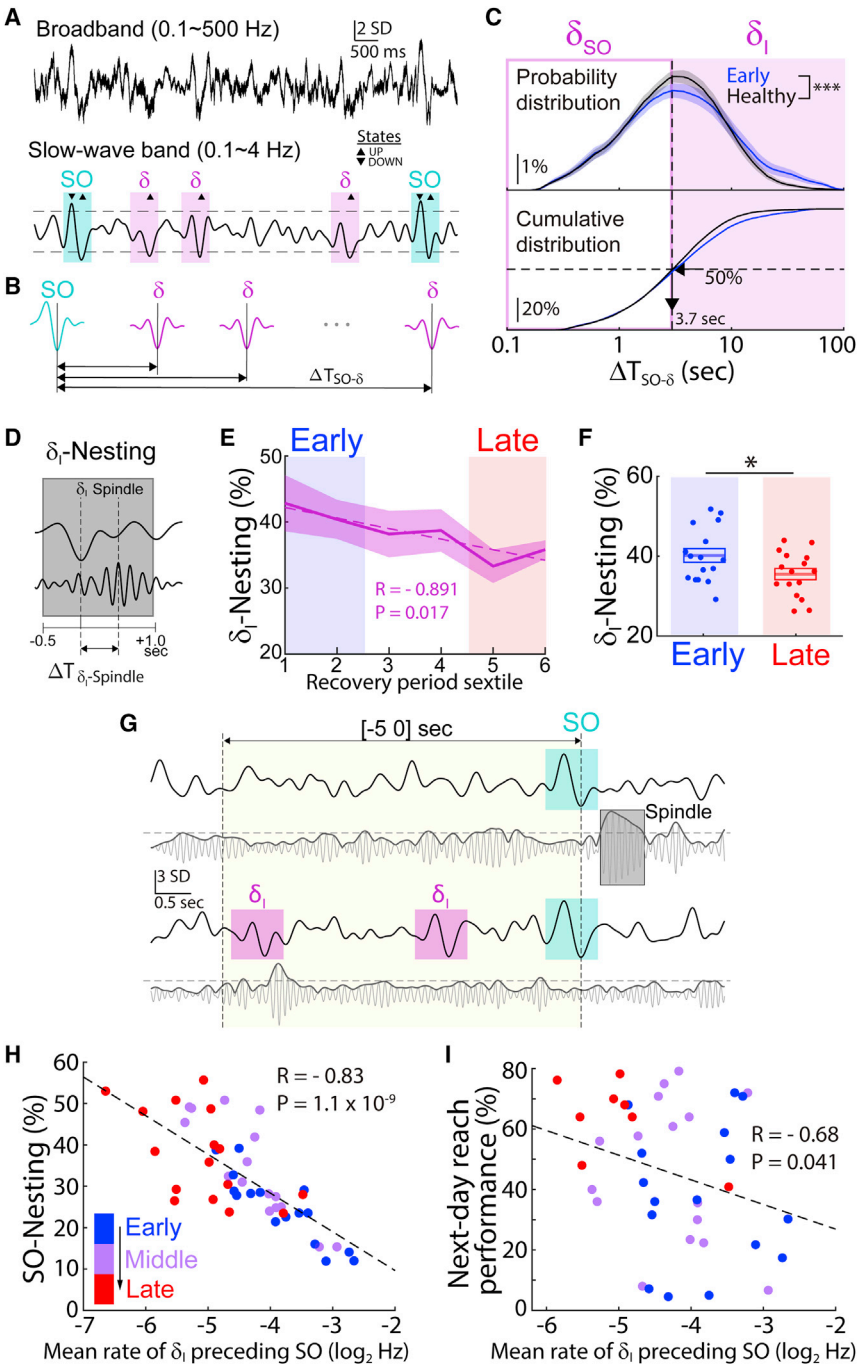

Figure 3. Pathological increase of δ_I

(A) Examples of broadband (0.1–500 Hz) and filtered (0.1–4 Hz).

(B) Schematic showing the temporal distance of δ waves from SO ($\Delta T_{SO-\delta}$).

(C) Comparison of SO-coupled δ (δ_{SO}) and isolated δ (δ_I) for early stroke (blue; n = 16 sessions, eight rats) and healthy (black; n = 9 sessions, five rats; Kolmogorov-Smirnov test [KS] statistic = 0.17, $^{***}p < 10^{-15}$). Average distributions of $\Delta T_{SO-\delta}$ are shown. δ_{SO} and δ_I waves were separated by the 50th percentile (3.7 s, vertical dashed line) from the distribution of healthy.

(D) Cartoon of nesting of spindle to δ_I (δ_I nesting).

(E) δ_I nesting over recovery (n = 8 rats). Dashed is linear regression (R = −0.891; p = 0.017). Mean ± SEM.

(F) Comparison of δ_I nesting between early versus late (early, n = 16 sessions in eight rats, 40.1% ± 1.7% versus late, n = 16 sessions in eight rats, 35.4% ± 1.4%, LME, $t_{30} = -2.27$, *p = 0.031; using average per period, early, n = 8 rats, 40.1% ± 2.3% versus late, n = 8 rats, 35.4% ± 1.7%, LME, $t_{14} = -1.74$, **p = 0.10). Mean ± SEM.

(G) Top: LFP traces filtered at slow-wave band and spindle band (case where no δ_I wave preceded SO during −5–0 s from an SO up state (yellow box). Bottom: same in a case where two δ_I waves preceded SOs −5–0 s from an SO up state is shown.

(H) Relationship between the mean rate of δ_I waves preceding SOs within 5 s and the SO nesting over all recovery sextiles. There was a negative correlation (n = 48 sessions in eight rats, six pairs per animal; dashed line, LME fit, R = −0.83, $p = 1.1 \times 10^{-9}$).

(I) Relationship between the mean rate of δ_I waves preceding SOs within 5 s to the next-day reach performance. There was a negative correlation (n = 40 sessions in eight rats, five pairs per animal; LME fit, R = −0.68, p = 0.041).

Strikingly, treatment with the drug resulted in significantly stronger SO-spindle nesting with a concomitant reduction in δ_I spindle nesting (Figure 4B). Notably, drug infusion in a separate group of healthy animals resulted in stronger δ_I spindle nesting with non-significant changes in SO spindle nesting (Figure S3; SO nesting: sham, n = 9 sessions in three rats, 28.4% ± 0.73% versus drug, n = 9 sessions in three rats, 26.8% ± 1.7%, LME, $t_{16} = -1.14$, p = 0.27; δ_I nesting: sham, 35.2% ± 1.1% versus drug, 38.7% ± 1.3%, LME, $t_{16} = 3.59$, $p < 10^{-2}$). This suggests that the beneficial effect of the drug is specific for stroke$_{exp}$ and perhaps detrimental in healthy animals (see discussion). In stroke$_{exp}$ animals, we also observed increased excitability; the unit MD during SO was stronger (Figure 4C). Moreover, changes in the unit MD during spindles, a measure of the effectiveness of spindles in modulating local spiking, could be explained by an increase in SO nesting (Figure 4D). We did not find any differences for the ET-1 and PT groups (ET-1 versus PT; ΔSO nesting: two-sample t test, $t_{15} = -0.14$, p = 0.89; Δspindles-MD: two-sample t test, $t_{15} = -0.064$, p = 0.95). Notably, for SO-spindle nesting and δ_I-spindle nesting, sham showed significant differences compared with the baseline, i.e., drop in SO-spindle nesting and increase in δ_I-spindle nesting after stroke$_{exp}$, while the drug was not significantly different from the baseline (SO nesting: sham versus baseline, LME, $t_{13} = 3.93$, $p = 1.7 \times 10^{-3}$, drug versus baseline, LME, $t_{13} = 2.01$, p = 0.067; δ_I nesting: sham versus baseline, LME, $t_{13} = -3.09$, $p = 8.6 \times 10^{-3}$, drug versus

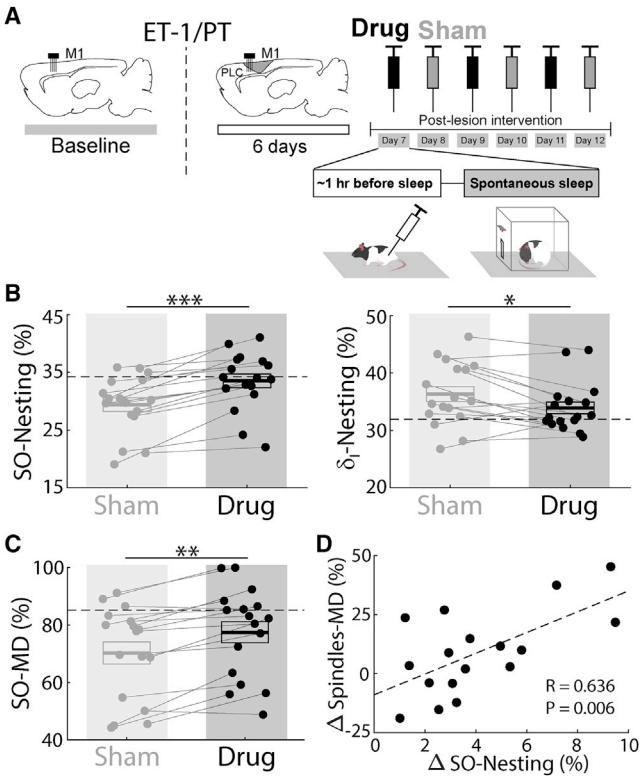

Figure 4. Blocking $GABA_A$ α5-subtype receptor increases SO nesting

(A) LFP/spike was monitored in PLC (n = 6 rats). Either ET-1 (n = 3) or PT (n = 3) was induced. In ET-1, LFP/spike activity was recorded 2 to 3 days before inducing $stroke_{exp}$ (vertical dashed line) for baseline. Either L655-708 (drug) or saline (sham) was administrated intraperitoneally (i.p.) on separate days.

(B) Comparison of SO nesting and δ_l nesting. SO nesting and δ_l nesting was stronger and weaker, respectively, with drug compared with sham (SO nesting: sham, n = 17 sessions, 29.4% ± 1.2% versus drug, n = 17 sessions, 33.5% ± 1.2%, LME, $t_{32} = 6.93$, ***$p < 10^{-7}$; δ_l nesting: sham, 36.3% ± 1.3% versus drug, 33.9% ± 1.0%, LME, $t_{32} = -2.29$, *p = 0.028). Baseline in horizontal dashed line is shown. Mean ± SEM.

(C) Comparison of unit MD during SO (SO-MD: sham, 70.3% ± 3.8% versus drug, 77.5% ± 3.7%, LME, $t_{32} = 2.79$, **p < 0.01). Mean ± SEM.

(D) Relationship of change of SO nesting in (B) to MD during spindles. There was a positively significant correlation (LME fit; R = 0.636; p = 0.006).

baseline, LME, $t_{13} = -1.55$, p = 0.15). Thus, our results indicate that elevated $GABA_A$-mediated tonic inhibition can alter the sleep microarchitecture.

DISCUSSION

Our results suggest a roadmap to delineate normal versus pathological sleep after stroke; they also suggest novel therapeutic targets to modulate sleep processing (e.g., tonic GABA and SO-spindle nesting) in order to enhance recovery (Figure S4).

Sleep and memory consolidation post-stroke

Electroencephalogram (EEG) studies in patients (Macdonell et al., 1988; Poryazova et al., 2015; Tu-Chan et al., 2017; van Dellen et al., 2013) and LFP recordings in animal models (Carmichael and Chesselet, 2002; Gulati et al., 2015) have found increased low-frequency power during awake periods. These studies have indicated that this increased low-frequency power is a marker of cortical injury and loss of subcortical inputs (Topolnik et al., 2003). Our findings of increased local δ_l waves are perhaps related to this phenomenon. Importantly, the increased frequency of δ_l waves preceding SOs was closely associated with the attenuated coupling of spindles to SOs (Figure 3H). We further found evidence for normalization of SO-δ_l interactions with recovery and task training.

In general, there is growing evidence that the temporal couplings of spindles to SOs are essential drivers of memory consolidation during sleep (Antony et al., 2018; Cairney et al., 2018; Helfrich et al., 2018; Kim et al., 2019; Latchoumane et al., 2017; Maingret et al., 2016; Staresina et al., 2015). Such coupling has been linked to spike-time-dependent plasticity (Bergmann and Born, 2018). It is also a potent driver of the reactivation of awake experiences (Antony et al., 2018; Cairney et al., 2018; Ngo et al., 2013; Peyrache et al., 2009). Finally, disruption of this coupling has been found to impair memory consolidation after awake experiences (Kim et al., 2019). Thus, our results suggest a link between pathological changes in network physiology after $stroke_{exp}$ to impaired sleep-associated processing, primarily via disruption of precise spindle-SO coupling. It is important to note that our observations of changes in sleep microstructure during recovery are largely correlational at this stage.

Implications for rehabilitation

We found that changes in sleep processing after $stroke_{exp}$ were correlated with offline gains during recovery. Importantly, clinical rehabilitation approaches are quite varied and not simply equal to task training; moreover, there are differences in training that aim to restore function as opposed to enabling compensation (Bernhardt et al., 2017; Ganguly et al., 2013; Pearson-Fuhrhop et al., 2009). Even so, our reach training offers a way to study functional recovery in both rodents and non-human primates (Guo et al., 2021; Khanna et al., 2021; Ramanathan et al., 2018; Whishaw et al., 1986). Based on this, our results specifically suggest that marking whether sleep is pathological or physiological may be an important consideration for timing rehabilitation. Interestingly, past studies in humans and rodents have suggested a sensitive period in which training can trigger long-term benefits (Dromerick et al., 2009, 2021; Krakauer et al., 2012). Notably, if it is indeed the case that awake low-frequency power in stroke patients is related to our observed effects on sleep processing, it might help explain past results indicating that awake low-frequency power is a predictor of recovery. EEG studies can also delineate when and if the transition to physiological sleep occurs and whether this is related to the sensitive period.

Implications for therapeutic neuromodulation

Our results have implications for translational studies. Animal studies have suggested that $GABA_A$-mediated tonic inhibition in the PLC may be a therapeutic target to promote recovery; blockade of $GABA_A$-mediated tonic inhibition was found to promote motor recovery maximally within the first 1 or 2 weeks in mice (Clarkson et al., 2010; He et al., 2019). Both short-term

(i.e., acutely prior to training) and long-term chronic infusion have been tested. Intriguingly, long-term infusion appears to be better (Clarkson et al., 2010). Although our pharmacological experiments were performed in a separate group of animals without motor training, our results provide a possible mechanism for why long-term infusion by Clarkson and colleagues may be essential to achieve prominent benefits; more specifically, the effect of this drug might not only help with task-specific online training, i.e., encoding motor skills during awake training, but also promote offline memory consolidation during sleep.

Our results also suggest possible approaches to neuromodulation to enhance recovery. It is quite likely that SOs and δ waves can be monitored using EEG recordings in stroke patients. Moreover, non-invasive brain stimulation during sleep (Antony et al., 2018; Cairney et al., 2018; Marshall et al., 2006; Ngo et al., 2013) can be tailored based on suppressing δ waves or enhancing SOs. It is also possible that invasive approaches for neuromodulation after stroke (Levy et al., 2016) can also focus on optimizing sleep processing. For example, while recent studies have shown that direct electrical stimulation can enhance awake performance after $stroke_{exp}$ (Khanna et al., 2021; Ramanathan et al., 2018), there has been less of a focus on extending this to sleep periods. Interestingly, a recent study suggested that neuromodulation to modulate up states during sleep can enhance recovery (Facchin et al., 2020). It is quite possible that closed-loop neuromodulation approaches that focus on both optimizing task performance and its consequence during sleep processing (Kim et al., 2019) may lead to the greatest long-term benefits during rehabilitation.

Limitations of the study

A limitation of this study is that it is difficult for us to distinguish the effect of a deficient capacity of encoding during awake training from our observed changes in sleep processing and offline gains following sleep. For example, it is likely that, with recovery, more effective task performance and associated ensemble dynamics (Guo et al., 2021; Khanna et al., 2021; Ramanathan et al., 2018) also influence the efficacy of sleep processing. However, it is worth pointing out that precise manipulations of sleep processing in healthy animals are sufficient to prevent offline gains even when awake task learning was robust. For example, our recent study found that relatively precise modulation of the extent of sleep spindle-SO coupling in healthy animals could either enhance or impede sleep processing (Kim et al., 2019). Future studies using such precise modulation approaches can causally test whether manipulation of sleep processing after $stroke_{exp}$ is sufficient to enhance or impede motor recovery.

Another limitation of this study is the $stroke_{exp}$ model and the time course of recovery. Our approach of using the focal M1 stroke model was to more precisely map out the network consequence of an injury. A future study using more extensive lesions (e.g., occlusion of the middle cerebral artery) that span multiple areas would be able to further investigate principles of recovery during sleep. This may also be more fruitful in a non-human primate model (Khanna et al., 2021; Nudo et al., 1996), where sensorimotor networks are more extensive and compartmentalized. Lastly, the pharmacological experiments were performed during the spontaneous recovery without motor training. By combining motor task training and drug manipulation, future work can better define the causal role of drug manipulation during sleep in motor recovery after stroke.

STAR★METHODS

Detailed methods are provided in the online version of this paper and include the following:

- KEY RESOURCES TABLE
- RESOURCE AVAILABILITY
  - Lead contact
  - Materials availability
  - Data and code availability
- EXPERIMENTAL MODEL AND SUBJECT DETAILS
- METHOD DETAILS
  - Animals/surgery
  - Photothrombotic and endothelin-1 induced focal $stroke_{exp}$
  - Electrophysiology
  - Behavior
  - $GABA_A$ α5-subtype receptor inverse agonist treatment
  - Analyses across-session versus within-session
  - Identification of NREM sleep waves
  - Spindle nesting analyses
  - Spike activity during sleep waves
- QUANTIFICATION AND STATISTICAL ANALYSIS

SUPPLEMENTAL INFORMATION

Supplemental information can be found online at https://doi.org/10.1016/j.celrep.2022.110426.

ACKNOWLEDGMENTS

Research was supported by awards from the Department of Veterans Affairs, Veterans Health Administration (VA Merit: 1I01RX001640 to K.G.; VA CDA to D.S.R., 7IK2BX003308); NCIRE; the Weill Neurohub, The National Institute of Neurological Disorders and Stroke (5K02NS093014 to K.G.; K99NS119737 to J.K.); American Heart Association Postdoctoral Fellowship (831442 to J.K.); and the Basic Science Research Program through the National Research Foundation of Korea (2018R1A6A3A03013031 to J.K.). K.G. and D.S.R. hold a Career Award for Medical Scientists from the Burroughs Wellcome Fund.

AUTHOR CONTRIBUTIONS

J.K., L.G., D.S.R., S.-J.W., and K.G. conceived and designed the experiments. J.K., L.G., A.H., S.L., and S.-J.W. conducted the experiments. J.K. analyzed all data, L.G. analyzed the data for Figure 1B, and A.H. analyzed the data for Figures 2D and 2E. J.K. and K.G. wrote and edited the manuscript.

DECLARATION OF INTERESTS

The authors declare no competing interests.

Received: July 2, 2021
Revised: November 1, 2021
Accepted: February 1, 2022
Published: March 1, 2022

REFERENCES

Aarts, E., Verhage, M., Veenvliet, J.V., Dolan, C.V., and van der Sluis, S. (2014). A solution to dependency: using multilevel analysis to accommodate nested data. Nat. Neurosci. *17*, 491–496.

Antony, J.W., Piloto, L., Wang, M., Pacheco, P., Norman, K.A., and Paller, K.A. (2018). Sleep spindle refractoriness segregates periods of memory reactivation. Curr. Biol. *28*, 1736–1743.e1734.

Backhaus, W., Braass, H., Gerloff, C., and Hummel, F.C. (2018). Can daytime napping assist the process of skills acquisition after stroke? Front. Neurol. *9*, 1002.

Baumann, C.R., Kilic, E., Petit, B., Werth, E., Hermann, D.M., Tafti, M., and Bassetti, C.L. (2006). Sleep EEG changes after middle cerebral artery infarcts in mice: different effects of striatal and cortical lesions. Sleep *29*, 1339–1344.

Bergmann, T.O., and Born, J. (2018). Phase-amplitude coupling: a general mechanism for memory processing and synaptic plasticity? Neuron *97*, 10–13.

Bernardi, G., Siclari, F., Handjaras, G., Riedner, B.A., and Tononi, G. (2018). Local and widespread slow waves in stable NREM sleep: evidence for distinct regulation mechanisms. Front Hum. Neurosci. *12*, 248.

Bernhardt, J., Hayward, K.S., Kwakkel, G., Ward, N.S., Wolf, S.L., Borschmann, K., Krakauer, J.W., Boyd, L.A., Carmichael, S.T., and Corbett, D. (2017). Agreed definitions and a shared vision for new standards in stroke recovery research: the stroke recovery and rehabilitation roundtable taskforce. Int. J. Stroke *12*, 444–450.

Born, J., Rasch, B., and Gais, S. (2006). Sleep to remember. Neuroscientist *12*, 410–424.

Burns, B.D. (1951). Some properties of isolated cerebral cortex in the unanaesthetized cat. J. Physiol. *112*, 156.

Burns, B.D., and Webb, A.C. (1979). The correlation between discharge times of neighbouring neurons in isolated cerebral cortex. Proc. R. Soc. Lond. Ser. B Biol. Sci. *203*, 347–360.

Buzsáki, G. (2015). Hippocampal sharp wave-ripple: a cognitive biomarker for episodic memory and planning. Hippocampus *25*, 1073–1188.

Cairney, S.A., Guttesen, A.A.V., El Marj, N., and Staresina, B.P. (2018). Memory consolidation is linked to spindle-mediated information processing during sleep. Curr. Biol. *28*, 948–954.e944.

Carmichael, S.T., and Chesselet, M.F. (2002). Synchronous neuronal activity is a signal for axonal sprouting after cortical lesions in the adult. J. Neurosci. *22*, 6062–6070.

Clarkson, A.N., Huang, B.S., Macisaac, S.E., Mody, I., and Carmichael, S.T. (2010). Reducing excessive GABA-mediated tonic inhibition promotes functional recovery after stroke. Nature *468*, 305–309.

de Vivo, L., Bellesi, M., Marshall, W., Bushong, E.A., Ellisman, M.H., Tononi, G., and Cirelli, C. (2017). Ultrastructural evidence for synaptic scaling across the wake/sleep cycle. Science *355*, 507–510.

Dromerick, A.W., Geed, S., Barth, J., Brady, K., Giannetti, M.L., Mitchell, A., Edwardson, M.A., Tan, M.T., Zhou, Y., Newport, E.L., et al. (2021). Critical Period after Stroke Study (CPASS): a phase II clinical trial testing an optimal time for motor recovery after stroke in humans. Proc. Natl. Acad. Sci. U S A *118*, e2026676118.

Dromerick, A.W., Lang, C.E., Birkenmeier, R.L., Wagner, J.M., Miller, J.P., Videen, T.O., Powers, W.J., Wolf, S.L., and Edwards, D.F. (2009). Very early constraint-induced movement during stroke rehabilitation (VECTORS) A single-center RCT. Neurology *73*, 195–201.

Duss, S.B., Seiler, A., Schmidt, M.H., Pace, M., Adamantidis, A., Muri, R.M., and Bassetti, C.L. (2017). The role of sleep in recovery following ischemic stroke: a review of human and animal data. Neurobiol. Sleep Circadian Rhythms *2*, 94–105.

Egert, D., Pettibone, J.R., Lemke, S., Patel, P.R., Caldwell, C.M., Cai, D., Ganguly, K., Chestek, C.A., and Berke, J.D. (2020). Cellular-scale silicon probes for high-density, precisely localized neurophysiology (124: J. Neurophysiology), pp. 1578–1587.

Facchin, L., Schone, C., Mensen, A., Bandarabadi, M., Pilotto, F., Saxena, S., Libourel, P.A., Bassetti, C.L.A., and Adamantidis, A.R. (2020). Slow waves promote sleep-dependent plasticity and functional recovery after stroke. J. Neurosci. *40*, 8637–8651.

Ganguly, K., Byl, N.N., and Abrams, G.M. (2013). Neurorehabilitation: motor recovery after stroke as an example. Ann. Neurol. *74*, 373–381.

Gao, B., Cam, E., Jaeger, H., Zunzunegui, C., Sarnthein, J., and Bassetti, C.L. (2010). Sleep disruption aggravates focal cerebral ischemia in the rat. Sleep *33*, 879–887.

Genzel, L., Kroes, M.C., Dresler, M., and Battaglia, F.P. (2014). Light sleep versus slow wave sleep in memory consolidation: a question of global versus local processes? Trends Neurosci. *37*, 10–19.

Giubilei, F., Iannilli, M., Vitale, A., Pierallini, A., Sacchetti, M., Antonini, G., and Fieschi, C. (1992). Sleep patterns in acute ischemic stroke. Acta Neurol. Scand. *86*, 567–571.

Gottselig, J.M., Bassetti, C.L., and Achermann, P. (2002). Power and coherence of sleep spindle frequency activity following hemispheric stroke. Brain. *125*, 373–383.

Gulati, T., Guo, L., Ramanathan, D.S., Bodepudi, A., and Ganguly, K. (2017). Neural reactivations during sleep determine network credit assignment. Nat. Neurosci. *20*, 1277–1284.

Gulati, T., Ramanathan, D.S., Wong, C.C., and Ganguly, K. (2014). Reactivation of emergent task-related ensembles during slow-wave sleep after neuroprosthetic learning. Nat. Neurosci. *17*, 1107–1113.

Gulati, T., Won, S.J., Ramanathan, D.S., Wong, C.C., Bodepudi, A., Swanson, R.A., and Ganguly, K. (2015). Robust neuroprosthetic control from the stroke perilesional cortex. J. Neurosci. *35*, 8653–8661.

Guo, L., Kondapavulur, S., Lemke, S.M., Won, S.J., and Ganguly, K. (2021). Coordinated increase of reliable cortical and striatal ensemble activations during recovery after stroke. Cell Rep. *36*, 109370.

He, W.M., Ying-Fu, L., Wang, H., and Peng, Y.P. (2019). Delayed treatment of alpha5 GABAA receptor inverse agonist improves functional recovery by enhancing neurogenesis after cerebral ischemia-reperfusion injury in rat MCAO model. Sci. Rep. *9*, 2287.

Helfrich, R.F., Mander, B.A., Jagust, W.J., Knight, R.T., and Walker, M.P. (2018). Old brains come uncoupled in sleep: slow wave-spindle synchrony, brain atrophy, and forgetting. Neuron *97*, 221–230.

Ito, H.T., Zhang, S.J., Witter, M.P., Moser, E.I., and Moser, M.B. (2015). A prefrontal-thalamo-hippocampal circuit for goal-directed spatial navigation. Nature *522*, 50–55.

Khanna, P., Totten, D., Novik, L., Roberts, J., Morecraft, R.J., and Ganguly, K. (2021). Low-frequency stimulation enhances ensemble co-firing and dexterity after stroke. Cell *184*, 912–930.e920.

Kim, J., Gulati, T., and Ganguly, K. (2019). Competing roles of slow oscillations and delta waves in memory consolidation versus forgetting. Cell *179*, 514–526.e513.

Kim, J.K., and Fiorillo, C.D. (2017). Theory of optimal balance predicts and explains the amplitude and decay time of synaptic inhibition. Nat. Commun. *8*, 14566.

Klinzing, J.G., Niethard, N., and Born, J. (2019). Mechanisms of systems memory consolidation during sleep. Nat. Neurosci. *22*, 1598–1610.

Korman, M., Doyon, J., Doljansky, J., Carrier, J., Dagan, Y., and Karni, A. (2007). Daytime sleep condenses the time course of motor memory consolidation. Nat. Neurosci. *10*, 1206–1213.

Krakauer, J.W., Carmichael, S.T., Corbett, D., and Wittenberg, G.F. (2012). Getting neurorehabilitation right: what can be learned from animal models? Neurorehabil. Neural Repair *26*, 923–931.

Latchoumane, C.F.V., Ngo, H.V.V., Born, J., and Shin, H.S. (2017). Thalamic spindles promote memory formation during sleep through triple phase-locking of cortical, thalamic, and hippocampal rhythms. Neuron *95*, 424–435.

Lemke, S.M., Ramanathan, D.S., Darevksy, D., Egert, D., Berke, J.D., and Ganguly, K. (2021). Coupling between motor cortex and striatum increases during sleep over long-term skill learning. Elife *10*, e64303.

Levy, R.M., Harvey, R.L., Kissela, B.M., Winstein, C.J., Lutsep, H.L., Parrish, T.B., Cramer, S.C., and Venkatesan, L. (2016). Epidural electrical stimulation for stroke rehabilitation: results of the prospective, multicenter, randomized, single-blinded everest trial. Neurorehabil. Neural Repair *30*, 107–119.

Macdonell, R.A., Donnan, G.A., Bladin, P.F., Berkovic, S.F., and Wriedt, C.H. (1988). The electroencephalogram and acute ischemic stroke. Distinguishing cortical from lacunar infarction. Arch. Neurol. *45*, 520–524.

Maingret, N., Girardeau, G., Todorova, R., Goutierre, M., and Zugaro, M. (2016). Hippocampo-cortical coupling mediates memory consolidation during sleep. Nat. Neurosci. *19*, 959–964.

Marshall, L., Helgadottir, H., Molle, M., and Born, J. (2006). Boosting slow oscillations during sleep potentiates memory. Nature *444*, 610–613.

Molle, M., Yeshenko, O., Marshall, L., Sara, S.J., and Born, J. (2006). Hippocampal sharp wave-ripples linked to slow oscillations in rat slow-wave sleep. J. Neurophysiol. *96*, 62–70.

Ngo, H.-V.V., Miedema, A., Faude, I., Martinetz, T., Mölle, M., and Born, J. (2015). Driving sleep slow oscillations by auditory closed-loop stimulation—a self-limiting process. J. Neurosci. *35*, 6630–6638.

Ngo, H.V., Martinetz, T., Born, J., and Molle, M. (2013). Auditory closed-loop stimulation of the sleep slow oscillation enhances memory. Neuron *78*, 545–553.

Nita, D.A., Cisse, Y., Timofeev, I., and Steriade, M. (2007). Waking-sleep modulation of paroxysmal activities induced by partial cortical deafferentation. Cereb. Cortex *17*, 272–283.

Norrving, B., and Kissela, B. (2013). The global burden of stroke and need for a continuum of care. Neurology *80*, S5–S12.

Nudo, R.J., Wise, B.M., SiFuentes, F., and Milliken, G.W. (1996). Neural substrates for the effects of rehabilitative training on motor recovery after ischemic infarct. Science *272*, 1791–1794.

Pack, A.I., Galante, R.J., Maislin, G., Cater, J., Metaxas, D., Lu, S., Zhang, L., Von Smith, R., Kay, T., Lian, J., et al. (2007). Novel method for high-throughput phenotyping of sleep in mice. Physiol. Genomics *28*, 232–238.

Pearson-Fuhrhop, K.M., Kleim, J.A., and Cramer, S.C. (2009). Brain plasticity and genetic factors. Top. Stroke Rehabil. *16*, 282–299.

Peyrache, A., Khamassi, M., Benchenane, K., Wiener, S.I., and Battaglia, F.P. (2009). Replay of rule-learning related neural patterns in the prefrontal cortex during sleep. Nat. Neurosci. *12*, 919–926.

Poryazova, R., Huber, R., Khatami, R., Werth, E., Brugger, P., Barath, K., Baumann, C.R., and Bassetti, C.L. (2015). Topographic sleep EEG changes in the acute and chronic stage of hemispheric stroke. J. Sleep Res. *24*, 54–65.

Ramanathan, D.S., Gulati, T., and Ganguly, K. (2015). Sleep-dependent reactivation of ensembles in motor cortex promotes skill consolidation. PLoS Biol. *13*, e1002263.

Ramanathan, D.S., Guo, L., Gulati, T., Davidson, G., Hishinuma, A.K., Won, S.J., Knight, R.T., Chang, E.F., Swanson, R.A., and Ganguly, K. (2018). Low-frequency cortical activity is a neuromodulatory target that tracks recovery after stroke. Nat. Med. *24*, 1257–1267.

Robinson, M.J., Macrae, I.M., Todd, M., Reid, J.L., and McCulloch, J. (1990). Reduction of local cerebral blood flow to pathological levels by endothelin-1 applied to the middle cerebral artery in the rat. Neurosci. Lett. *118*, 269–272.

Roome, R.B., Bartlett, R.F., Jeffers, M., Xiong, J., Corbett, D., and Vanderluit, J.L. (2014). A reproducible Endothelin-1 model of forelimb motor cortex stroke in the mouse. J. Neurosci. Methods *233*, 34–44.

Rothschild, G., Eban, E., and Frank, L.M. (2017). A cortical-hippocampal-cortical loop of information processing during memory consolidation. Nat. Neurosci. *20*, 251–259.

Sarasso, S., D'Ambrosio, S., Fecchio, M., Casarotto, S., Vigano, A., Landi, C., Mattavelli, G., Gosseries, O., Quarenghi, M., Laureys, S., et al. (2020). Local sleep-like cortical reactivity in the awake brain after focal injury. Brain *143*, 3672–3684.

Sharkey, J., Ritchie, I.M., and Kelly, P.A. (1993). Perivascular microapplication of endothelin-1: a new model of focal cerebral ischaemia in the rat. J. Cereb. Blood Flow Metab. *13*, 865–871.

Siengsukon, C.F., and Boyd, L.A. (2009). Sleep to learn after stroke: implicit and explicit off-line motor learning. Neurosci. Lett. *451*, 1–5.

Silversmith, D.B., Lemke, S.M., Egert, D., Berke, J.D., and Ganguly, K. (2020). The degree of nesting between spindles and slow oscillations modulates neural synchrony. J. Neurosci. *40*, 4673–4684.

Sirota, A., Csicsvari, J., Buhl, D., and Buzsaki, G. (2003). Communication between neocortex and hippocampus during sleep in rodents. Proc. Natl. Acad. Sci. U S A *100*, 2065–2069.

Staresina, B.P., Bergmann, T.O., Bonnefond, M., van der Meij, R., Jensen, O., Deuker, L., Elger, C.E., Axmacher, N., and Fell, J. (2015). Hierarchical nesting of slow oscillations, spindles and ripples in the human hippocampus during sleep. Nat. Neurosci. *18*, 1679–1686.

Stickgold, R. (2005). Sleep-dependent memory consolidation. Nature *437*, 1272–1278.

Tononi, G., and Cirelli, C. (2014). Sleep and the price of plasticity: from synaptic and cellular homeostasis to memory consolidation and integration. Neuron *81*, 12–34.

Topolnik, L., Steriade, M., and Timofeev, I. (2003). Partial cortical deafferentation promotes development of paroxysmal activity. Cereb. Cortex *13*, 883–893.

Tu-Chan, A.P., Natraj, N., Godlove, J., Abrams, G., and Ganguly, K. (2017). Effects of somatosensory electrical stimulation on motor function and cortical oscillations. J. Neuroeng Rehabil. *14*, 113.

van Dellen, E., Hillebrand, A., Douw, L., Heimans, J.J., Reijneveld, J.C., and Stam, C.J. (2013). Local polymorphic delta activity in cortical lesions causes global decreases in functional connectivity. Neuroimage *83*, 524–532.

Virley, D., Hadingham, S.J., Roberts, J.C., Farnfield, B., Elliott, H., Whelan, G., Golder, J., David, C., Parsons, A.A., and Hunter, A.J. (2004). A new primate model of focal stroke: endothelin-1-induced middle cerebral artery occlusion and reperfusion in the common marmoset. J. Cereb. Blood Flow Metab. *24*, 24–41.

Walker, M.P., Brakefield, T., Morgan, A., Hobson, J.A., and Stickgold, R. (2002). Practice with sleep makes perfect: sleep-dependent motor skill learning. Neuron *35*, 205–211.

Whishaw, I.Q., Oconnor, W.T., and Dunnett, S.B. (1986). The contributions of motor cortex, nigrostriatal dopamine and caudate-putamen to skilled forelimb use in the rat. Brain. *109*, 805–843.

Wong, C.C., Ramanathan, D.S., Gulati, T., Won, S.J., and Ganguly, K. (2015). An automated behavioral box to assess forelimb function in rats. J. Neurosci. Methods *246*, 30–37.

Xia, F., Richards, B.A., Tran, M.M., Josselyn, S.A., Takehara-Nishiuchi, K., and Frankland, P.W. (2017). Parvalbumin-positive interneurons mediate neocortical-hippocampal interactions that are necessary for memory consolidation. Elife *6*, e27868.

Yang, G., Lai, C.S., Cichon, J., Ma, L., Li, W., and Gan, W.B. (2014). Sleep promotes branch-specific formation of dendritic spines after learning. Science *344*, 1173–1178.

Yizhar, O., Fenno, L.E., Prigge, M., Schneider, F., Davidson, T.J., O'Shea, D.J., Sohal, V.S., Goshen, I., Finkelstein, J., Paz, J.T., et al. (2011). Neocortical excitation/inhibition balance in information processing and social dysfunction. Nature *477*, 171–178.

STAR★METHODS

KEY RESOURCES TABLE

REAGENT or RESOURCE	SOURCE	IDENTIFIER
Chemicals, peptides, and recombinant proteins		
Rose bengal	Sigma-Aldrich	CAS# 330000
Endothelin-1	Sigma-Aldrich	CAS# 117399-94-7
L655,708	Sigma-Aldrich	CAS# 130477-52-0
Experimental models: Organisms/strains		
Long Evans Rat	Charles River Labs	Strain Code 006
Software and algorithms		
Offline Sorter v4.6.0	Plexon Inc	https://plexon.com/products/offline-sorter
SpikePac	Tucker-Davis Technologies (TDT)	https://www.tdt.com/support/downloads/
MATLAB R2020a	Mathworks	https://www.mathworks.com/products/matlab.html
SO, δ-waves, and spindles detection algorithms	Zenodo	https://doi.org/10.5281/zenodo.5911914
Other		
32-channel microwire electrode arrays	Tucker-Davis Technologies (TDT)	https://www.tdt.com/component/zif-clip-array-electrodes/
32-channel microwire electrode arrays	Innovative Neurophysiology Inc	http://www.inphysiology.com/optogenetic-applications/
128-channel custom electrode arrays	Egert et al., 2020	https://wwwabstractsonlinecom/pp8/#!/4649/presentation/24873
RHD 128-Channel recording headstage	Intan Technologies	https://intantech.com/RHD_headstages.html?tabSelect=RHD128ch
Infusion cannula	P1 Technologies	Cat# C315GS Cat# C235G

RESOURCE AVAILABILITY

Lead contact

Further information and requests for resources and reagents should be directed to and will be fulfilled by the lead contact, Karunesh Ganguly (karunesh.ganguly@ucsf.edu).

Materials availability

This study did not generate new unique reagents.

Data and code availability

- All data reported in this paper will be shared by the lead contact upon request.
- All original code has been deposited at Zenodo and is publicly available as of the date of publication. DOIs are listed in the key resources table.
- Any additional information required to reanalyze the data reported in this work paper is available from the lead contact upon request.

EXPERIMENTAL MODEL AND SUBJECT DETAILS

Experiments were approved by the Institutional Animal Care and Use Committee at the San Francisco VA Medical Center. We used a total of twenty eight adult Long-Evans male rats (250–400 g; Charles River Laboratories); twenty six rats with focal experimental stroke ($stroke_{exp}$) and two rats without $stroke_{exp}$ (Table S1; detailed contributions of each rat on the respective results). No statistical methods were used to predetermine sample sizes, but our sample sizes are similar to those reported in previous publications (Gulati

et al., 2014, 2017; Guo et al., 2021; Kim et al., 2019). Animals were kept under controlled temperature and a cycle with 12-h light and 12-h dark (lights on at 06:00 a.m.). Animals were pair-housed prior to electrode/cannula implantation and then singly housed after to prevent damage to implants. If applicable, animals were randomly assigned to experimental groups.

METHOD DETAILS

Animals/surgery

Surgeries were performed under isofluorane (1–3%) anesthesia and body temperature was maintained at 37°C with a heating pad. Atropine sulfate was also administered intraperitoneal/IP before anesthesia (0.02 mg/kg of body weight). We implanted 32/128-channel microwire arrays for recording LFP/spike activity; arrays were lowered down to 1,400–1,800 μm in layer 5 of the primary motor cortex (M1) or perilesional cortex (PLC) in the upper limb area. In the healthy animals (n = 2), neural probes were centered over the forelimb area of M1, at 3 mm lateral and 0.5 mm anterior from the bregma. In the stroke$_{exp}$ animals (n = 14), the neural probe was placed immediately anterior to the lesion site, typically centered ~3–4 mm anterior and 2.5–3 mm lateral to the bregma. The reference wire was wrapped around a screw inserted in the midline over the cerebellum. The final localization of depth was based on the quality of recordings across the array at the time of implantation. The post-operative recovery regimen included administration of buprenorphine at 0.02 mg/kg and meloxicam at 0.2 mg/kg. Dexamethasone at 0.5 mg/kg and trimethoprim sulfadiazine at 15 mg/kg were also administered postoperatively for 5 days. All animals were allowed to recover for at least five days with the same regimen as described above before the start of experiments. Data collection and analysis were not performed blind to the conditions of the experiments.

Photothrombotic and endothelin-1 induced focal stroke$_{exp}$

We used either photothrombotic (PT) and Endothelin-1 (ET-1) induced stroke$_{exp}$ models (see stroke$_{exp}$ types for each group of animals in Table S1). For the PT stroke$_{exp}$ model, rose bengal dye was injected into a femoral vein using and an intravenous catheter after craniotomy. Next, the surface of the brain was illuminated with white light (KL-1500 LCD, Schott) using a fiber optic cable for 20 min. We used a 4-mm aperture for stroke$_{exp}$ induction (centered in the M1 area based on stereotactic coordinates; −1.5–2.5 mm anterior and 1–5 mm lateral from the bregma) and covered the remaining cortical area with a custom aluminum foil mask to prevent light penetration. After induction, a probe was implanted in the PLC immediately anterior to the lesion site (Gulati et al., 2015; Ramanathan et al., 2018). The craniotomy and implanted electrodes were covered with a layer of low toxicity silicone adhesive (WPI KWIK-SIL), then covered by dental cement. For the precise measure of baseline of LFP/spike activity before inducing stroke$_{exp}$ (pre-stroke$_{exp}$ baseline in Figure 4A), we also used ET-1 induced focal stroke$_{exp}$ model (Robinson et al., 1990; Roome et al., 2014; Sharkey et al., 1993; Virley et al., 2004) in three rats (Figure 4). To induce ET-1 stroke$_{exp}$, microarray attached with infusion cannula (guide: 26G; internal: 33G; P1 Technology) was implanted into the M1 area; single cannula in one rat and bilateral cannula with 2 mm spacing in the other two rats. The cannula was centered at 3 mm lateral and 0.5 mm anterior from the bregma to target M1 and microarray was positioned anterior to the cannula; the lesion site and recording site were targeted to correspond to the PT stroke$_{exp}$ animals. The remaining operation procedures were the same as the PT stroke$_{exp}$ animals. The ET-1 induced stroke$_{exp}$ model allowed us to induce the focal stroke$_{exp}$ following a baseline measurement; after measuring baseline spike/LFP activity for 2 days, ET-1 was injected with 1.5 ul through a single cannula in one rat, and a total 2.0 ul (two sites injections; 1.0 ul for each) through a bilateral cannula (100 nL per min) in the other two rats into deep cortical layers (1.4 mm from the surface of the brain). We then measured spike/LFP activity during the recovery period following the ET-1 stroke$_{exp}$ induction.

Electrophysiology

We conducted AC-coupled recordings and recorded extracellular neural activity using 32-channel microwire electrode arrays (MEAs; 33-μm-length, 250-μm-spacing, 4-rows, standard polyimide-coated tungsten microwire arrays from Tucker-Davis Technologies (TDT) for ten rats; 25-μm-length, 200-μm-spacing, 6-rows, tungsten microwire arrays from Innovative Neurophysiology Inc. for five rats) and 128-channel custom electrode arrays (Egert et al., 2020) (for one rat). All electrode arrays showed similar quality of LFP (e.g., LFP amplitude and noise level). The microwire arrays from Innovative Neurophysiology Inc. were customized so that a cannula is placed beside the recording sites of microwires. We recorded spike and LFP activity using a 128-channel RZ2 bioamp processor (TDT) and 128-channel neurodigitizer (digital PZ4 or PZ5).

Spike data was sampled at 24,414 Hz and LFP data at 1,018 Hz. ZIF-clip-based headstages (TDT) for 32-channel microwires and SPI-based headstates (RHD 128-Channel Recording Headstage, Intan Technologies) for 128-channel microwire with a unity gain and high impedance (~1 G) was used. Only clearly identifiable units with good waveforms and a high signal-to-noise ratio were used. The remaining neural data (e.g. filtered LFP) was recorded for offline analysis at 1,018 Hz. Behavior-related timestamps (that is, trial onset and trial completion) were sent to the RZ2 analog input channel using a digital board and then used to synchronize to neural data in the offline analyses. Electrophysiology was not monitored during the baseline sessions illustrated for the pre-stroke$_{exp}$ motor performance in Figure 1 and in the animal group of Figure 2D (see Table S1 for the corresponding animals).

Behavior

After recovery, animals were typically handled for several days before the start of experimental sessions, i.e., "motor training sessions." Animals were acclimated to a custom plexiglass behavioral box during this period without motor training. The box was

equipped with a door at one end. We examined two groups of stroke$_{exp}$ animals; with motor training in Figures 1, 2, and 3 and with spontaneous recovery in Figure 4. In the rats used for Figure 4 (testing the effect of reducing tonic GABA$_A$), animals experienced spontaneous recovery without motor training. In the other rats of Figures 1, 2, and 3, animals were trained to a plateau level of performance in a reach-to-grasp single-pellet task before neural probe implantation or PT stroke$_{exp}$ induction (baseline; pre-stroke$_{exp}$ training period in Figure 1A). In a single session of the motor training post-stroke$_{exp}$, pre-training sleep, reach training, post-training sleep, and reach retrieval blocks were monitored in sequence. We measured relative reach performance, i.e., pellet retrieval success rate in the reach-to-grasp task, using normalized metrics relative to the baseline, Figure 1B; PT stroke$_{exp}$ impaired motor performance (baseline, n = 16 sessions in 8 rats: 100 ± 1.9% vs. early, n = 16 sessions in 8 rats: 47.8 ± 6.8%; LME, $t_{30} = -7.44$, $P < 10^{-7}$). It improved over the subsequent training (late, n = 16 sessions in 8 rats: 75.4 ± 4.7%; early vs. late, LME, $t_{30} = 5.78$, $P < 10^{-5}$). However, the absolute reach performance was compared to sleep metrics for all other analyses. The reach-to-grasp task has been used as a sensitive measure of motor function; it requires reaching, grasping, and retrieving a single pellet located at a distance outside of the behavior box (Figure S1A) (Guo et al., 2021; Ramanathan et al., 2018; Whishaw et al., 1986; Wong et al., 2015). Probe implantation and stroke$_{exp}$ induction were performed contralateral to the preferred hand. Animals were allowed to rest at least for 6 days before the start of motor training or recording sessions post-stroke$_{exp}$. The stroke$_{exp}$ animal group experienced motor training until the motor performance reached a plateau level of performance (motor performance in an individual animal is shown in Figure S1D), which is called motor training post-stroke$_{exp}$ during the recovery period in Figure 1A. The first reach training session for the "across-session" analyses was between the 7–14th day (9.1 ± 2.6, mean ± s.d.); this was because of the need to restart food scheduling. Each animal was monitored for 6–11 sessions/days until a stable plateau was reached (Figure S1B). Given the variability of recovery times, and as described in the results, sessions per animal were divided into tertiles and termed 'early', 'middle' and 'late.' During behavioral assessments, we monitored the animals and ensured that their body weights did not drop below 90% of their initial weight. We monitored electrophysiology, i.e., LFP/spike only during the pre-training sleep, reach training, post-training sleep, and retrieval period of each session, not during 24 h of a single day. This typically totaled a period of 4–5 h a day in the behavior box. After completing motor tasks and sleep sessions in the behavioral box, animals were placed in the home cage without electrophysiology monitoring.

For the behavioral task, we used an automated reach-box, controlled by custom MATLAB scripts and an Arduino microcontroller. This setup for the reach-to-grasp task required minimal user intervention, as described previously (Wong et al., 2015). Each trial consisted of a pellet dispensed on the pellet tray, followed by a beep indicating that the trial was beginning; this was followed by the door opening. Animals then had to reach their arm out, grasp and retrieve the pellet. A real-time "pellet detector" using an infrared detector centered over the pellet was used to determine when the pellet was moved, which indicated that the trial was over and the door was closed. All trials were captured by video, which was synced with the electrophysiology data using the Arduino digital output. The video frame rate was 30 Hz for six animals and 75 Hz for two animals. The reach performance (the number of accurate pellet retrieval/the total number of trials x 100%) was determined manually from a recorded video. The reach performance was used not only as a measure of motor function recovery across sessions (Figure 1B) but also as a measure of "*offline gains*" that may be the result of memory consolidation from sleep (Figure 2C). As a measure of offline gain, we computed the next-day reach performance (i.e., a change in reach performance between Day X reach training and the following Day X+1 reach training; Figure 2C) and the within-session changes (i.e., reach performance changes after post-training sleep compared to before post-training sleep, Figure 2E). These measurements allowed us to quantify offline gains and motor recovery either across sessions and within a session (see also below). For the sleep restriction experiments, i.e., no-sleep group in Figure 2D, moderate vibration on the behavior box was given when rats were not active for >40 s, to prevent from sleeping. In this restriction group (n = 8 rats), sleep was deprived either 2 or 6 h after the training and then the retrieval was conducted (n = 4 restricted for 2 h; n = 4 restricted for 6 h).

GABA$_A$ α5-subtype receptor inverse agonist treatment

Treatment with the GABA$_A$ α5-subtype receptor inverse agonist (L655,708; "drug" condition in Figure 4) was initiated 6 days after ET-1 stroke$_{exp}$ induction; previous studies reported that L655,708 promoted functional recovery 7 days after stroke$_{exp}$ (Clarkson et al., 2010; He et al., 2019). About 0.5–1 h before sleep onset, rats received intraperitoneal/IP injections of vehicle (i.e., saline as the "sham") or L655,708 (Sigma-Aldrich; 5 mg/kg, dissolved in dimethylsulphoxide/DMSO and then diluted 1:1 in 0.9% saline as the "drug" condition). Over the course of 6 days, we used either sham or drug every other day (see experiment flow in Figure 4A). To counterbalance the starting condition between sham and drug conditions in six animals, either drug or sham was administrated IP on separate days, i.e., the drug condition was tested every other day during range of day 7–12. The starting condition was the drug at day 7 in three rats and the sham at day 7 in the other three rats. More precisely, the sham was conducted on days 7, 9, and 11 for ET-1 induced animals (n = 3), and the drug was conducted on days 7, 9, and 11 for PT induced animals (n = 3).

Analyses across-session versus within-session

In the stroke$_{exp}$ experiment in Figures 1, 2, and 3, animals performed the reaching task during recovery (6–11 days of training). For long-term recovery in the stroke$_{exp}$ animal group, we specifically analyzed the "pre-training sleep" and the "reach training" over a ~3 weeks recovery period. In the other experiment, to test the effect of reducing tonic GABA$_A$ in Figure 4, we focused on spontaneous

changes in sleep microarchitectures without motor training over a ~2 weeks recovery period. These analyses of the changes over a long-term recovery period are termed "across-session" analyses. In each animal, the 1–2 weeks recovery period was divided into sextiles and a representative session in each sextile was used. The motor performance and the sessions used are marked in Figures S1B. In five animals, all monitored sessions were used (i.e., two sessions per period and total of six sessions were monitored). In three animals, representative sessions (two sessions per period) were selected in order to balance the number of sessions per animal, e.g., typically every other session was selected. In Figure 2, we also compared sleep metrics within a single-day session/experiment (i.e., "within-session" analyses). Sleep metrics (e.g., SO-Nesting) were measured as a pair of pre-training and post-training sleep in a single-day session, then the change from the pre-training to the post-training sleep was computed (e.g., ΔSO-Nesting). These metrics (e.g., Day X) were then compared with the offline gains in motor performance during the reach training of the following day (e.g., Day X+1) in Figure 2C. In Figures 2D and 2E, the within-session offline gains in motor performance (i.e., changes from reach training to reach retrieval within a single session) were examined.

Identification of NREM sleep waves

LFP activity was recorded using 32/128-channel microwire electrode arrays (see above). The LFP was analyzed after removing obvious artifacts (>10 s.d.) and excluding bad channels. Identification of NREM epochs was performed by classification based on power spectral density of the LFP. LFP trace was segmented into non-overlapping 6-s epochs. In each epoch, the power spectral density was computed and averaged over the slow-wave frequency band including SO and δ-waves (0.1–4 Hz, also called Delta band) and Gamma frequency bands (30–60 Hz). Then a k-means classifier was used to classify epochs into two clusters, NREM sleep and REM/awake; REM sleep and awake were not classified and NREM sleep was focused on in this study. Sleep epochs less than 30 s were excluded from NREM sleep epochs. The identified NREM sleep durations were not different between the early period and late period of motor recovery (Figure S1D). The identified NREM sleep epochs were verified by visual assessment of the LFP activity. During the NREM period with high Delta power (0.1–4 Hz), strong down- and up-states dominates. Thus, we assessed if our detected NREM sleep epochs contain a high-amplitude and slow LFP fluctuation distinguished from a low-amplitude and high-frequency LFP during the awake period. Moreover, we assessed if there were substantial missing detections of NREM sleep epoch; assessment if a high amplitude LFP epoch was not included in the detected NREM sleep epochs excessively. These power-based sleep detections showed a close match to the video-based detections (Kim et al., 2019; Pack et al., 2007) (Figure S1C); the number of pixels that changed intensity frame to frame in each pair of consecutive frames was computed from a recorded video (1 Hz frame rate using Microsoft LifeCam Cinema Webcam) during the sleep block; these values were then integrated over an epoch of 40 s. If that integrated value was higher than a threshold, that epoch was identified as sleep; the threshold was chosen by comparing detection results and visual assessment of the recorded video.

In offline analysis, SO, δ-waves and spindles were detected using the algorithm used in previous studies (Gulati et al., 2017; Kim et al., 2019; Lemke et al., 2021; Silversmith et al., 2020). The LFP average across all recording channels excluding bad channels was filtered in the SO/δ band (0.1–4 Hz) through two independent filterings; the high pass Butterworth filter (second order, zero phase-shifted, with a cutoff at 0.1 Hz) was applied and then followed by the low pass Butterworth filter (fifth order, zero phase-shifted, with a cutoff at 4 Hz). The individual order of the high-pass and low-pass filter was estimated through a conventional minimum-order design; it required to meet maximum passband ripple of 3 dB and minimum stopband (presumed 0.02 Hz for high-pass filter and 6 Hz for low-pass filter) attenuation of 15 dB. Next, all positive-to-negative zero crossings during NREM sleep were identified, along with the previous peaks, the following troughs, and the surrounding negative-to-positive zero crossings. Then the positive threshold (the top 15 percentile of the peaks) and the negative threshold (the bottom 40 percentile of the troughs) were respectively defined for the down-states and up-states; in Figure 1C, horizontal dashed lines indicate the threshold detecting SO up/down states. Each identified wave was considered an SO if the trough was lower than the negative threshold (i.e., up-state), the peak preceding that up-state was higher than the positive threshold (i.e., down-state), and the duration between the peak and the trough was between 150 ms and 500 ms (Figures 1C and 3A). On the other hand, a slow wave was considered a δ-wave if the trough was lower than the negative threshold (i.e., up-states) and that the up-state was preceded by a maximum voltage that was lower than the positive threshold within 500 ms. In this study, we separated δ-waves into two classes (SO-coupled/δ_{SO} and isolated/δ_{I}) depending on their temporal interaction with a preceding SO, i.e., $\Delta T_{SO\text{-}\delta}$ (Figures 3B and 3C). This distinction was based on simply dividing the $\Delta T_{SO\text{-}\delta}$ distributions using the 50_{th} percentile; δ-waves less than the 50^{th} percentile were labeled δ_{SO}, whereas the remaining δ-waves were labeled δ_{I}. $\Delta T_{SO\text{-}\delta} > 100$ s (1–2%) were manually removed to exclude the cases driven by the possible error in NREM sleep detections; this error was evaluated by visual inspection of slow-wave activity. From the distribution of $\Delta T_{SO\text{-}\delta}$ in healthy brains (n = 9 sessions, 5 rats), 50^{th} percentile of $\Delta T_{SO\text{-}\delta}$ (3.7 s) was set as the cutoff separating δ-waves into "δ_{SO}" and "δ_{I}" waves; δ-waves within the close 50% from a preceding SO ($\Delta T_{SO\text{-}\delta} \leq 3.7$ s) were labeled "δ_{SO}," whereas δ-waves of the distal 50% from a preceding SO ($\Delta T_{SO\text{-}\delta} > 3.7$ s) were labeled "δ_{I}." The cutoff of $\Delta T_{SO\text{-}\delta}$ determined by the healthy conditions was also used for $stroke_{exp}$ conditions. The distribution of $\Delta T_{SO\text{-}\delta}$ was more variable across the $stroke_{exp}$ animals; it appears to be due to the variability of lesion size. Specifically in the comparison with the same animal, the distribution of $\Delta T_{SO\text{-}\delta}$ after $stroke_{exp}$ appeared to be abnormal compared to the healthy condition without $stroke_{exp}$ (n = 1 rat; Kolmogorov-Smirnov test, KS-statistic = 0.18, $^{***}P < 10^{-9}$). Therefore, the cutoff of $\Delta T_{SO\text{-}\delta}$ was determined by using the healthy conditions.

For spindles detection, the LFP was first z-scored in each channel and averaged across all good channels. The LFP average was filtered in spindle band (10–15 Hz) through two independent zero phase-shifted filterings (Figures 1C and 3A); the high pass

Butterworth filter (sixth order, zero phase-shifted, with a cutoff at 10 Hz) was applied and then followed by the low pass Butterworth filter (eighth order, zero phase-shifted, with a cutoff at 15 Hz). The individual order of the high-pass and low-pass filter was estimated through a conventional minimum-order design; it required to meet maximum passband ripple of 3 dB, and minimum stopband (presumed 7 Hz for high-pass filter and 19 Hz for low-pass filter) attenuation of 15 dB. We computed a smoothed envelope of this signal, the magnitude of the Hilbert transforms with convolving by a Gaussian window (200 ms). Next, we determined two thresholds for spindle detection based on the mean (μ) and standard deviation (σ) of the spindle band LFP during NREM sleep; the upper and lower thresholds were set $\mu + 2.5 \times \sigma$ and $\mu + 1.5 \times \sigma$, respectively; in Figure 1C, horizontal dashed lines indicate the threshold detecting spindle period. Epochs in which the spindle power exceeded the upper threshold for at least one sample and the spindle power exceeded the lower threshold for at least 500 ms were considered spindles. Each epoch where the spindle power exceeded the lower threshold was considered the start and stop of the spindle; the duration of each spindle was based on these values as well.

Spindle nesting analyses

We also analyzed the temporal coupling of spindles relative to SO or δ-waves. For the nesting of spindles to SO (SO-Nesting; Figure 1D), each spindle was linked to the closest SO. The time difference between the peak of the spindle and the up-state of the linked SO was measured for each detected spindle ($\Delta T_{SO\text{-}Spindle}$). If $\Delta T_{SO\text{-}Spindle}$ was between -0.5 s and 1.0 s (i.e., nesting time window), that spindle event was considered an SO-nested spindle. In this study, we also focused on the temporal interaction of spindles to the δ_l-waves. Thus, the nesting of spindles to δ_l (δ_l-Nesting; Figure 3D) was identified in a manner analogous to the "SO-Nesting" value, i.e., time differences between the spindle peak time and the time of the δ_l up-state. To quantitatively assess the changes in the temporal coupling of spindles to SO, we specifically measured as the following; time lag of spindle from the closest SO ($\Delta T_{SO\text{-}Spindle}$) was measured for each spindle event and the rate of spindles of which $\Delta T_{SO\text{-}Spindle}$ was within the nesting time window was measured; i.e., the number of SO-nested spindles/the total number of spindles $\times$ 100% (Figures 1G and 1H). We also measured δ_l-Nesting the same way as the "SO-Nesting" but using time lags between the peaks of spindles and the up-states of the linked δ_l; i.e., the number of δ_l-nested spindles/the total number of spindles $\times$ 100% (Figures 3E and 3F).

Spike activity during sleep waves

We initially used an online sorting program (SpikePac, TDT). We then conducted offline sorting using Plexon Inc's Offline Sorter. Only clearly identifiable units with good waveforms and a high signal-to-noise ratio were used. To assess spike activity modulation during sleep oscillations, we analyzed peri-event time histogram (PETH) and unit modulation-depth (MD). After spikes were time-locked to event reference times (e.g., SO up-states or SO-nested spindles), the PETH (bin length 20 ms) was estimated. Then, the unit MD was calculated by comparing the difference between maximum and minimum of the PETH around events time (SO-MD: within -0.5 to 0.3 s from SO up-states; spindles-MD: -0.25 to 0.15 s from spindles peaks) over the baseline firing activity (averaged activity within -2 to -0.5 s from the events for both SO-MD and spindles-MD); i.e., (maximum-minimum)/baseline firing rate. In other words, the MD is a measure of the modulation of firing rate relative to the pre-event start baseline rate. This was compared for the early period and the late period of recovery in Figure 1I and for the sham and drug conditions in Figures 4C and 4D. No significant change in population spike rates was found from the early to the late period (early vs. late, mixed-effects model, $t_{97} = -0.29$, $P = 0.77$).

QUANTIFICATION AND STATISTICAL ANALYSIS

Figures show mean $\pm$ s.e.m.; if this was not the case, we specifically indicated it. Parametric statistics were generally used in this study (linear mixed-effects model (LME), t-tests, linear regression, Pearson's correlation otherwise stated); they were implemented within MATLAB. A "hierarchical nested statistics approach" of LME (using the MATLAB function "fitlme") was used for the comparison of task performance, temporal coupling of spindles, unit MD, and linear relationship (Aarts et al., 2014; Guo et al., 2021; Khanna et al., 2021; Kim et al., 2019). This was done to account for the repeated measures per animals; thus, this statistical approach ensured that the group level statistc accounted for sessions per animal and did not treat them as statistically independent samples. We fit random effects (e.g., rats) specified as an intercept for each group and reported fixed effects representing population parameters to compare (e.g., early vs late period). Adding random effects to a model recognizes correlations within sample subgroups (e.g., rat) and extends the reliability of inferences beyond the variability across multiple rats. The fixed effects were tested for p values of the linear regression slope coefficients associated with two comparing conditions. In this way, the LME accounts for the fact that units, sessions, events, or experimental conditions from the same animal are more correlated than those from different animals and is more stringent than computing statistical significance over all units, sessions, events, and conditions. The LME was used to compare $stroke_{exp}$ versus healthy conditions, early period versus late period, sham versus drug, and sleep versus no-sleep. The used random effects and fixed effects parameters are following; Figures 1H, 1I, 2B, 3F, S1D, and S2, random: rat, fixed: recovery period; Figure 2D, random: rat, fixed: sleep type; Figures 4B and 4C, random: rat, fixed: injection type. In these figures, the mean in each experiment session was used as the response parameter and two categories of the comparing conditions were used as the predictor parameter.

LME was also used to evaluate linear relationships or correlations between the changes in SO-Nesting and the next-day task performance in Figure 2C, between the post-training sleep duration and the within-session changes of task performance in Figure 2E,

between the mean rate of δ_l preceding SO and the SO-Nesting in Figure 3H, between the mean rate of δ_l preceding SO and the next-day task performance in Figure 3I, and between the changes of SO-Nesting and the changes in spindles-MD in Figure 4D. We also used traditional linear regression or correlation to evaluate the relationship between the recovery period and the sleep metrics (e.g. SO-Nesting and δ_l-Nesting) in Figures 1G, 3E, and S2 left. For the comparison between distributions, we used Kolmogorov-Smirnov's test in Figure 3C to test the samples were drawn from the same distribution and Bartlett's test in Figure 1F to test equal variances (sharpness of distribution) between early period and late period.